Table of Contents

AN Fe-12Ni-4Co-2Mo-.05Ti ALLOY FOR USE AT 77°K AND BELOW

Bradley Watford Whitaker

Inorganic Materials Research Division, Lawrence Berkeley Laboratory and Department of Materials Science and Engineering, College of Engineering; University of California, Berkeley, California

ABSTRACT

A variant of the maraging class of steels is proposed for application at 77°K and below where a combination of very high strength and good toughness is required. The alloy has a composition of Fe-12Ni-4Co-2Mo-0.05Ti with low interstitial content.

The as quenched and quenched and aged structures were completely martensitic with a prior austenitic grain size of 10-12 μm. This structure had a Y.S. of 138.5 ksi and 154 ksi before and after aging respectively. All aging was done at 444°C for 4 hours. The DBTT was shown to lie above 77°K as measured by C_v testing.

Based on dilotometric studies of the $\alpha \rightarrow \gamma$ and $\gamma \rightarrow \alpha$ transformation temperatures a cycling treatment consisting of reportedly heating to above the A_f temperature followed by a water quench was utilized to further reduce the prior γ grain size to $\sim$4-6 μm. The structure was completely martensitic and possessed a Y.S. of 151 ksi at 77°K in the unaged condition with a $Y.S./K_{IC}$ ratio of 1.9 while the aged structure showed a Y.S. of 162 ksi with a $Y.S./K_{IC}$ ratio of 1.3. C_v testing showed the DBTT to lie between 77°K and 4.2°K.

Further grain refinement was accomplished by a 2 phase decomposition procedure which resulted in a grain size of 1-2 μm. The structure which contained decreasing amounts of austenite with temperature

(3.0% at R.T. to 1.0% at 4.2°K) showed the best combination of strength and ductility at 4.2°K. A Y.S. of 205 ksi with a Y.S./K_{IC} ratio of 0.84 was achieved before aging. The aged structure was brittle at 4.2°K with a Y.S. of 218 ksi and a Y.S./K_{IC} ratio of 0.425.

ACKNOWLEDGMENTS

I wish to express my deep gratitude and special thanks to Professor J. W. Morris Jr. for the many helpful discussions we had concerning this work. I would further like to thank Dr. S. Jin for his support during this study, and Madaleine Penton and Shirley Ashley who are directly responsible for the lack of "typos" in this thesis.

This work was supported by the U. S. Energy Research and Development Administration.

I. INTRODUCTION

Almost thirty years after its inception by G. R. Brophy and A. J. Miller[1] 9Ni steel remains the primary ferritic steel in commercial use for temperatures down to as low as 77°K. This steel offers the excellent strength normally associated with B.C.C. materials (nearly twice the yield strength of 304 S.S. at 77°K) while maintaining adequate ductility. It is a quench and temper steel and thus lends itself to simple and economical fabrication procedures. For a discussion of the role of nickel steels in LNG tankers see Reference 2 and for a compilation of cryogenic alloys along with the tensile properties of each see Reference 3.

Most work on cryogenic ferritic steels has been performed on 9Ni steel,[4,5,6] with little attention given to the development of new high strength alloys suitable for use at temperatures down to 4.2°K. These low temperatures are below the lower limit of usefulness for 9Ni steel. The development of high strength alloys for use in this temperature regime has become especially desirable since the discovery of the phenomenon of superconductivity.

Recent work performed at this institution has shown Fe-12Ni-Ti alloys to possess an excellent combination of strength and ductility at 77°K.[7] Further work on an Fe-12Ni-0.25Ti alloy showed an excellent combination of strength and ductility at temperatures down to 4.2°K when the alloy was subjected to a two phase decomposition procedure to produce an extremely fine grain size of approximately 1 μm.[8,9,10] Table 1 compares the two most popular cryogenic alloys with the Fe-12Ni-0.25Ti alloy in the grain refined (G.R.) condition.

The work presented here is an attempt to develop an alloy with superior strength and toughness to those alloys listed in Table 1. Special emphasis was given to properties at 4.2°K. The only restriction placed upon this work at the outset was the prohibition of thermo-mechanical processes in favor of pure thermal treatment to effect the desired properties. It was then decided to concentrate upon B.C.C. iron based alloys because of the high strength obtainable with the B.C.C. matrix. No particular emphasis is placed upon economy in either alloy composition or alloy processing. No consideration was given to possible fabrication procedures.

A. Alloy Design Considerations

It is of primary importance when attempting to promote excellent toughness characteristics in a high strength ferritic matrix to adhere to the following general rules.

i) Utilize a matrix which approaches optimum dislocation mobility and cross slip characteristics consistent with strength requirements.

ii) Minimize grain size - reduction in grain size is the single clearly demonstrable parameter which simultaneously increases strength while promoting resistance to unstable crack propagation.

iii) Avoid coarse ppt. in the matrix - decohesion at ppt./matrix interface or cleavage of hard ppt. particles result in:

a) premature void nucleation in ductile matrices

b) initiation of microcracks leading to unstable crack propagation in less ductile matrices.

iv) Avoid alloy segregation to or continuous ppt. at grain boundaries which might reduce the critical stress to cleave the boundaries resulting in a low energy intergranular fracture.

Nickel is the single known element which when added to iron lowers the Ductile/Brittle Transition Temperature (DBTT) by fundamentally affecting the slip characteristics of the matrix. Although the exact role of Ni in this respect is not known it is known that the addition of Ni to Fe reduces the temperature at which a transformation occurs from cross (wavy) slip, characteristic of high temperatures, to planar slip associated with low temperatures.[11] Ni also reduces the dependence of the yield strength on temperature and strain rate.[12] The Ni-Fe matrix exhibits a highly dislocated massive martensitic structure when Ni is present in the range of 6% to 25%.[13] Such massive martensitic structures are conducive to high strength, good ppt. dispersion characteristics for those ppt. which are dislocation nucleated, and good transformation characteristics since the optimum structure is produced by air quenching.

The heat treatments used here were chosen because they represent proven techniques for the refinement of grain size in the absence of mechanical processing. G. Saul, et al.,[14] presented a method of refining prior austenitic grains in an Fe-Ni matrix (250 and 300 grade maraging steels) by repeated cycling of the material into the γ region. S. Jin, et al.,[9] were abel to attain grain sizes down to approximately

.5 μm diameter by successive two phase decompositions which utilize a diffusion controlled austenitic reversion reaction.

The temperature needed to effect austenite reversion in a reasonable time during 2 phase decomposition (to grain refine) has been shown to promote overaged precipitates (presumably Ni_3Ti) in an Fe-12Ni-0.25Ti alloy. Ti is added primarily as a "gettering" element to remove interstitials (primarily C and N but also possibly O) from solution through the formation of Ti(C,N).[15,16,17] It is expected that the Ti in excess of that needed to rid the matrix of interstitials takes part in this precipitation reaction. Based on an expected maximum interstitial content of 100 ppm (by wt.) a Ti content of 0.05% is sufficient to scavenge the matrix.

Co (Fe, Ni, Ti, Mo) precipitation has never been observed in an iron based alloy. Co additions of up to 8% (by wt.) in a 10Ni, low C iron alloy was shown to effect a small solid solution hardening reaction, retardation of dislocation recovery at ~450°C, retardation of austenite reversion, and a reduction in the amount of austenite present at equilibrium.[18]

Mo when present with Co has been shown to be a unique couple in high Ni iron matrix of the maraging steels. A fine evenly dispersed Mo-Ni precipitate (commonly agreed to be orthorhombic or hexagonal Ni_3Mo)[19,20,21] is nucleated on the dense dislocation network which the Co has helped to preserve at aging temperatures. The nature and/or morphology of this precipitation has been credited in part for the excellent combination of strength and toughness of maraging steels.

Mo additions promote toughness in some thermally embrittled steels. The reason for this is not clear but it has been suggested that Mo inhibits precipitation at, or alloy segregation to prior austenite grain boundaries.[22]

Because the maraging steels have historically exhibited an excellent combination of strength and toughness and in light of the above considerations it was decided to utilize a ppt. hardenable alloy patterned after the maraging steels. A 12Ni-Fe matrix was chosen as a base for historical reasons to which the Co-Mo couple was added. No data is available concerning aging kinetics or solubility limits in such alloys but based on available data from 18Ni-Fe systems,[23] a 4Co-Mo couple was found to be suitable.

The alloy presented here then has a 12Ni-4Co-2Mo-.05Ti-Fe composition. A 12Ni-.05Ti-Fe alloy was also tested and data from it is injected when needed to aid in discussion.

II. EXPERIMENTAL PROCEDURE

A. Material Preparation

The alloys employed in this investigation were all prepared at this facility using a 100 Kilowatt vacuum induction furnace. All elemental additions were of at least 99.9% purity. Melting was accomplished in an Argon atmosphere at a pressure of 200 mm of Hg after a double evacuation procedure (to 20 μm of Hg) coupled with a preheat to rid the system of non-inert gases. The melt was poured at approximately 1650°C into a rotating Cu chill mold and allowed to furnace cool over night. Table 2 shows the compositions of the ingots produced. The cylindrical ingots measured approximately 12 in. long and were of two types; a 23 lb. ingot which measured 2.75 in. in diameter and a 4 lb. ingot which measured 1.25 in. in diameter.

All ingots were homogenized at a temperature of 1200°C (2190°F ± 20°F) for 24 hrs. in a vacuum resistance type furnace at a pressure of approximately 5×10^{-4} mm of Hg. Cooling was accomplished by back filling the system with Argon gas down to 300°C and furnace cooling to room temperature.

The ingots were forged at approximately 1150°C (2100°F) in a single heat. The smaller type ingots were forged into slabs 1.7 in. × 0.5 in. × ℓ where the longitudinal axis of the slab was parallel to the longitudinal axis of the ingot (Fig. 1(a)). The larger type ingots were forged into slabs of dimension 2.0 in. × 0.75 in. × ℓ where the longitudinal axis of the slab was perpendicular to the longitudinal axis of the ingot (Fig. 1(b)). Comparison of the test results from these two configurations was based upon the fact that the microstructure

showed no preferred orientation in either case. The latter type of forging was performed to maximize the mechanical mixing of the ingot and further help to insure a chemically homogeneous material.

B. Heat Treatment

All test specimens were blanked from the forged ingots prior to heat treatment (H.T.) and machined subsequent to H.T. All heating except preliminary aging studies were performed in resistance type furnaces. No vacuum or special atmosphere was used for heats below 800°C. Above 800°C specimen blanks were enveloped in stainless steel bags to prevent excess oxidation. Preliminary aging studies were performed using a low temperature salt pot (molten cyanide salts) with temperature control accurate to ±1°C during any particular heat. The temperature control of the resistance type furnaces was accurate to ±2°C during any particular heat.

All specimen blanks for mechanical testing were heat treated at 900°C for 1 hr. and quenched to room temperature in agitated water to help insure an initially comparable microstructure subsequent to the various H.T. used here.

Fig. 2 shows a schematic of the H.T. used here. In general, three separate cycles were employed and an aging treatment was added to each, resulting in six distinct structures. The first two consisted of the 900°C/1 hr/W.Q. and the same structure aged at 444°C/4 hrs/A.Q. This corresponds to an as quenched and quenched and tempered structure, respectively. The second two structures are referred to as gamma cycled and gamma cycled and aged and correspond to the thermal cycling shown by

the dotted lines in Fig. 2 to which the aging treatment is added. The final two microstructures are referred to as grain refined and grain refined and aged. The G.R. structure consists of the γ cycled structure to which a double 2 phase decomposition is added as shown by the dashed lines in Fig. 2. Again, an additional aging treatment is added.

C. Dilotometry

Dilotometry studies were conducted to ascertain the phase transformation temperatures of the alloys considered here. Hollow cylindrical specimens were machined from material which had been air quenched from a 900°C/1 hr. treatment. The specimens were 1 cm. long, 0.5 cm outside diameter with a 1 mm wall thickness. The specimens were heated in air at a constant 10°C/min. up to 850°C, held for 20 min. and cooled to R.T. at approximately the same rate. Expansion and contraction characteristics of $\gamma \rightarrow \alpha$ and $\alpha \rightarrow \gamma$ shear transformations respectively were recorded with respect to temperature. The results can be seen in Table 3.

D. Mechanical Testing

1. Hardness Testing

Hardness tests were conducted using a Wilson Rockwell Hardness Tester and a "Brale" penetrator in conjunction with a 60 Kg load (A scale). A minimum of 4 readings were taken and an average value reported. Surface irregularities were removed in all cases by grinding on a 240 grit wet belt grinder.

2. Tensile Testing

The tensile test specimens used in this study are of the type shown in Fig. 3. The tests were conducted on an Instron Testing machine using a constant cross head speed of 0.05 cm/min. and a gage length of 0.5 in. resulting in a strain rate of 0.039/min. All yield strengths reported were generated from data using the 0.2% offset method except where noted.

Tests conducted at 77°K (-196°C) were performed by immersing the test specimen in $L.N_2$ during the test. An atmosphere of $L.He_2$ was used to generate data at 4.2°K.

3. Charpy Impact Testing

Charpy impact testing was performed using the specimen shown in Fig. 4 and test procedures according to ASTM E-23-64 except for C_v tests conducted at 4.2°K. The testing was conducted on a 225 ft-lb capacity machine with a hammer speed of 19.6 ft/sec. Data at 77°K were generated by immersing the specimen in $L.N_2$ prior to testing. Data at 4.2°K were generated using a technique developed in this lab.[24] All values reported are based upon the average of two tests.

4. Fracture Toughness Testing

Fig. 5 shows the configuration and dimensions of a standard compact tension specimen used in all F.T. testing presented here. All procedures followed correspond to ASTM E-399-72. Data at 77°K were generated by immersing the test specimen in $L.N_2$ during the testing. Data generated at 4.2°K were generated using a technique recently developed here in this lab.[10]

In all cases K_Q values were reported as per ASTM E-399-72. However, K_{IC} values were also calculated and presented based on the equivalent energy concept which strives to extend linear elastic fracture mechanics to the realm of elastic-plastic behavior.[25] The method was shown to have the ability to predict plane strain data based on elastic-plastic response in some cases.[26] The K_{IC} value is calculated as shown below:

$$K_{IC} = P_Q \frac{(A_1/A_2)^{1/2} f(a/w)}{B\sqrt{w}} \qquad (1)$$

where A_1 = area under load-COD curve to maximum load

A_2 = area under the curve to any point P_Q in the elastic region

$f(a/w)$ = geometrical factor available in ASTM E-399-72

B = specimen thickness

w = specimen width

a = crack length

E. X-Ray Diffraction

A Picker diffractometer (model 3488) was used to determine the volume percent of Austenite. A Cu tube was used at 40 kV and 14 ma with a LiF monochrometer (λ = 1.542Å).

Samples to be tested were specially heat treated for X-ray analysis or were cut from a non-load bearing section of a fracture toughness sp-cimen. The samples were ground to 4/0 emergy paper and chemically polished in a 5% HF-H_2O_2 solution for 3 min.

Samples were scanned from $2\theta = 70°$ to $2\theta = 95°$ to generate the $(220)_\gamma$, $(211)_\alpha$, and the $(311)_\gamma$ peaks. The volume percent austenite was calculated using the equation

$$V_\gamma = \frac{1.12\ I_\gamma}{I_\alpha + 1.12\ I_\gamma} \qquad (2)$$

where I_α = area under the $(211)_\alpha$ peak

I_γ = average value of the areas under the $(220)_\gamma$ and $(311)_\gamma$ peaks.

Values reported here are those calculated from equation (2) although they are valid only to ±5% in amounts as low as 2%. If no indication of a $(111)_\gamma$ peak was present ($2\theta = 43.7°$) an austenite free structure was reported.

F. Microscopy

1. Optical Microscopy

Where possible photomicrographs were taken from samples heat treated along with the test specimen blanks. Otherwise the samples were cut from mechanical test specimens.

The samples were mounted in Bakelite using a Struers hot press. Fine grinding was performed on emery paper in four steps down to 4/0 grade paper (~10 μm scratch size). Kerosene was used as a lubricant. The samples were polished using 1 μm diamond paste on a rotating wheel and 0.05 μm alumina in a vibrating slurry.

In all cases the specimens were first etched using a 5% picric acid solution in H_2O to which about 1 gm per 100 ml solution of Na

Dodecylbenzene sulfonate was added as a wetting agent. The samples were submerged in the etching solution and placed in an ultrasonic cleaner. Final etching was accomplished using a 2% nital solution applied with a swab.

Photographs were taken on a Zeiss 64559 metallograph using Polaroid type 55 positive/negative film. For magnifications in excess of 1000X oil immersion was used.

2. Scanning Electron Microscope

Fracture surfaces from selected Charpy and F.T. specimens were photographed using a Jeolco JSM-U3 microscope with secondary emissions at 25 kV.

3. Transmission Electron Microscopy

Foils suitable for examination were prepared using a standard Jet polishing technique. Samples were cut from specially heat treated specimens at approximately 0.030 in. in thickness. These samples were thinned to approximately 0.004 in. using a solution of 5% HF in H_2O_2. 2.3 mm discs were punched from the thinned samples and Jet polished using a solution of

77 gms	CrO_3
400 ml	Glacial Acetic
21 ml	H_2O

at approximately 25 volts.

TEM photomicrographs were taken on a Siemmens microscope using a 100 kV accelerating voltage. All photographs were taken at 20,000X magnification.

III. EXPERIMENTAL RESULTS AND DISCUSSION

A. Aging Reaction

Fig. 6 shows the result of extended aging times on this alloy. The curve for the 12Ni-Ti ternary is included for comparison. A temperature of 443°C was chosen because it lies at the lower boundary of the normal maraging temperature range. A low aging temperature was thought desirable for the following reasons:

i) to promote the retention of the high dislocation density and a finer precipitate dispersion

ii) to retard the formation of austenite due to 2 phase decomposition

iii) to increase the degree of supersaturation of Mo in Fe-12Ni matrix.

It is clear that the 4Co-2Mo alloy is stronger in the as quenched condition than the ternary alloy. This is most probably due to the solid solution strengthening effect of Mo.

Fig. 6 provides evidence of precipitation on this alloy. While the ternary alloy is decreasing in hardness the 4Co-2Mo alloy is slightly increasing in hardness.

The formation of metastable austenite at R.T. due to a low temperature aging treatment in the 2 phase region would invariably be associated with a rapid decrease in hardness.[28] No such rapid hardness decrease is present out to 150 hrs. Also, X-ray analysis confirmed the absence of any γ phase present at R.T. due to the 4 hr. aging treatment for both the quench and temper structure and the γ cycled and aged structure.

3. As Quenched and Quench and Temper Structure

Fig. 7 shows the microstructure of the 4Co-2Mo alloy in a quenched condition (a) and a quench and temper condition (b). (a) shows the massive martensitic structure normally associated with Fe-Ni-low C alloys in this range of Ni content. The structure is very "clean" and no precipitation or grain boundary decoration can be seen. (b) is identical to (a) except that some slight decoration of prior austenitic grain boundaries is noticeable. The reason for the selective etch attack at the grain boundaries is not known but may be due to the migration of free interstitials to the grain boundaries which represent areas of easier accomodation. Such effects were noted in work with Fe-12Ni binary alloys subjected to air cooling from the γ region. The decoration seemed to decrease as the Ti content increased.

The prior austenitic grain size can be seen from (b) to be approximately 10-12 μm in diameter.

Table 4 shows the tensile data for this structure tested at 77°K. The % Elong. and % R.A. both suggest excellent ductility at this temperature. However, Charpy V-notch tests conducted at 77°K showed an energy absorption of only 20 ft-lb for both structures. Fig. 8 shows the C_v fracture surface for both the quenched (a) and quench and temper (b) specimens. Both surfaces clearly show a predominantly transgranular cleavage fracture mode. The aged structure (b) showed cleaved facets approximately the size of the prior austenitic grain boundaries, while the unaged structure (a) did not show the same correlation. Clearly, the g.b. in the aged structure seem more effective in inhibiting unstable crack propagation.

77°K was judged to be below the DBTT and no further work was done on this structure.

C. Gamma Cycled and Gamma Cycled and Aged Structures

Fig. 9(a) shows the microstructure resulting from the treatment shown in Fig. 2 by the dotted lines. Fig. 9(b) is, again, the same structure but aged four hours at 443°C as shown in Fig. 2. The isolated areas of somewhat laminar morphology are most probably caused by partial reversion of γ at high temperatures just prior to and during the shear reaction $\alpha \rightarrow \gamma$. The γ phase nucleates at martensite lath boundaries,[29] and grows preferentially along those boundaries under the influence of enhanced Ni diffusion. Complete homogenization does not occur at 777°C due to the reduced diffusivity of Ni in F.C.C. γ iron.

The decoration of prior austenitic grain boundaries is again apparent as a result of aging. The size of the prior austenite grains can be seen to have been reduced to approximately 4-6 μm in diameter.

Fig. 10 and Fig. 11 show T.E.M. photomicrographs of the unaged and aged structures respectively, both of which are in the 100 orientation. A highly dislocated substructure consisting of lath martensite is apparent in both figures. Comparison of the two structures reveals little difference. However, in Fig. 11 there appear to be very small dark areas which seem to lie along the dislocations. Although no definite conclusions can be justified on the basis of these two photographs it is expected that these may be the dislocation nucleated precipitates reported for similar alloys. The lath size is seen to be

approximately 0.5 μm in width. No indication of a second phase was noted in the diffraction patterns.

Table 5 shows the tensile properties of the γ cycled structure in both conditions. Comparison of data for 77°K (Table 4) show that the γ cycling treatment increased both measures of strength by ~10 ksi with little if any sacrifice in % Elong. and % R.A. This can be attributed to a reduction in prior austenitic grain size. Table 5 clearly shows an increase in strength with decreasing temperature common to B.C.C. metals.

The results of C_v impact testing are given below.

C_v Energy (ft-lb), γ Cycled Structure

Condition	298°K	77°K	4.2°K
unaged	201.	152.	20.7
aged	206.	163.	16.5

It is clear that the DBTT lies between 77°K and 4.2°K. Fig. 12 shows the C_v fracture surface for both the unaged (a) and the aged structure tested at 77°K. Both surfaces exhibit dimple rupture fracture characteristic of an extremely high energy fracture. It is significant to note that aging results in a small increase in energy absorption for temperature above the DBTT.

On the basis of the C_v results presented above fracture toughness tests were conducted at 77°K and the results are presented in Fig. 13. While aging increased the toughness as measured by C_v testing, the F.T. tests showed a decrease in toughness with aging. These results show

that the aged structure has a K_{IC}/σ_y ratio of 1.3 which is excellent toughness at 162 ksi yield. Fig. 14 shows the fracture surfaces associated with the F.T. data. A quasi-cleavage fracture mode is apparent but here the facet size is approximately the same for both unaged (a) and aged (b) structures and generally corresponds to the prior austenitic grain size.

D. Grain Refined and Grain Refined and Aged Structures

Fig. 15 shows photomicrographs of the G.R. (a) and G.R. and aged (b) microstructures. A homogeneous structure has been approached, i.e., there is no indication of a preferred orientation in the overall structure. The grain size ranges from 0.5 μm to 5 μm but most seem to be from 1 to 2 μm.

1. X-Ray Analysis

Table 6 shows the results of quantitative analysis for austenite in a G.R. structure, unaged. All analyses were conducted at R.T. The samples were air cooled to R.T. where they remained during machining into test specimens. The data then refer to austenite present after reheating to R.T. from the temperatures noted. All samples were at the desired low temperature for a minimum of 3 min.

Since the G.R. structure is a γ cycled structure which has undergone a double 2 phase decomposition and no austenite was detected in the γ cycled structure we must conclude that the austenite reported in Table 6 is the untransformed high Ni γ phase generated in the 2 phase region. Fe-Ni austenite is unstable at R.T. in Ni concentrations less

than approximately 25% (wt.).[30] Based on Fe-Ni binary data, the Ni content of γ formed at 670°C is approximately 15% (wt.). Even allowing for a range in these values due to elemental additions to the Fe-Ni binary it is highly unlikely that the austenite reported is stable at R.T. and below.

R. L. Miller observed metastable austenite in a similar ultrafine grain Fe-Ni low carbon alloy which remained untransformed even to 4°K. Although this effect is unexplained, Miller proposed that the austenite was present due to a "compartmentalization" effect.[31]

In order to check the character of the austenite in this alloy a specially heat treated grain refined alloy was W.Q. to about R.T. and immediately quenched in L.N_2 and held for 12 hrs. No austenite was found after this treatment. The nature of this austenite, then, is different from that reported by Miller.

The behavior reported in Table 6 and described above can best be explained through a classic γ stabilization mechanism. Free interstitials act to pin dislocations in the α-γ interface (or in either phase) thus inhibiting the shear transformation.[32]

2. Mechanical Properties

Table 7 shows a tabulation of tensile data generated at R.T., 77°K, and 4.2°K. Comparison of this data with the data in Table 5 shows the G.R. structure to be less strong than the γ cycled structure when tested at 298°K and 77°K. This is in direct contradiction to the Hall-Petch relationship and known effects of grain refinement in similar alloys.[9] The reduced strength of the G.R. alloy may be the results of

metastable austenite present at the test temperatures. The comparative strength values at 4.2°K are consistent with the reduced amount of austenite at 4.2°K.

Fig. 16 shows a plot of yield strength and U.T.S. vs. temperature for both the unaged and aged structures. The rapid decrease in strength with increasing temperature characteristic of B.C.C. materials is clearly seen and is, in this case, augmented by the increase in the amount of austenite with increasing temperature.

Fig. 17 shows a graphical presentation of the results of Charpy impact testing at 298°K, 77°K, and 4.2°K. Clearly, 4.2°K is above the DBTT as measured by this test. Two facts can be seen from the graph, the first of which is the rather large scatter at lower temperatures. The second is that the data does not plot a straight line as would be expected above the DBTT. The concave upward shape of the plot may be due to the variation in γ present in the microstructure as a function of temperature.

Figs. 18-21 show the results of fracture toughness testing at 77°K and 4.2°K along with the fracture surfaces relative to each.

If Fig. 16 is compared to Fig. 11 and Table 7 is compared to Table 5 it can be noted that the K_{IC}/σ_y ratios for both the γ cycled and the G.R. structures in both unaged and aged conditions are greater than 1. All four structures are tough at 77°K. However, the high Y.S. of the γ cycled and aged structure gives it the best combination of strength and toughness.

Fig. 19 shows a quasi-cleavage fracture surface characteristic of a high energy fracture.

Fig. 20 shows the result of F.T. testing at approximately 4°K. The unaged specimen is tough at this temperature with a K_{IC}/σ_y ratio of .84. Note the shear lip in the macrofractograph. However, the aged specimen exhibits a K_{IC}/σ_y ratio of 0.44 and a flat fracture surface. Fig. 21 shows the microfracture surfaces. The unaged specimen (a) exhibits a rather fine quasi-cleavage structure while the aged specimen (b) shows much less dimple rupture and some indication of the riverlet pattern characteristic of transgranular cleavage.

E. Some Observations on the Effect of Aging

Fig. 22 shows a plot of Engr. stress vs. Engr. strain for this alloy in both the unaged and aged condition for the as quenched structure tested at 77°K. Three effects of aging can be seen and are listed below:

i) appearance of an upper and lower yield point

ii) increase in U.T.S.

iii) work hardening rate is increased.

The three effects can clearly be explained by the presence of a ppt. in the matrix. To check this further the ternary (Fe-12Ni-.01Ti) alloy was tested under the same conditions with the following results.

Unaged				Aged			
σ_y*	U.T.S.	% Elong.	% R.A.	σ_y	U.T.S.	% Elong.	% R.A.
118.5	132	33	73	128/127	135	36.5	75

*All values reported in ksi.

An upper and lower yield point also appeared but in an alloy presumably devoid of any precipitation. Clearly the 4Co-2Mo couple has little to do with the appearance of the yield point effect.

The U.T.S. seems to be increased less in the ternary alloy than in the 4Co-2Mo alloy as would be expected due to predipitation in the 4Co-2Mo alloy.

The rate of work hardening is increased less in the 4Co-2Mo alloy than in the ternary alloy. To the extent that the % Elong. reflects the rate of work hardening it is clear that a Mo-Ni ppt. has little to do with the increase in work hardening.

Further, the yield point effect due to aging was also noted for the γ cycled structure tested at 77°K and for the G.R. structure tested at both 77°K and 298°K. The yield point effect was not observed in the γ cycled and aged structure tested at R.T. Note that an upper and lower yield point was observed in the G.R. and aged structure even when aging at 444°C occurred subsequent to 1 hr. aging at 670°C. This suggests a low temperature effect.

A specially prepared tensile specimen was grain refined and aged at 444°C for 10 min. only. It was thought that if the yield point effect was caused by free interstitials the specially prepares specimen would also exhibit an upper and lower yield point. It did not.

On the basis of the observations above we can say that:

i) precipitation due to Mo-Ni during aging does not play a significant role in the appearance of an upper or lower yield point;

ii) precipitation due to Mo-Ni during aging does not play a significant role in the increase in work hardening;

iii) free interstitials do not contribute significantly to the formation of an upper or lower yield point.

Fig. 21 is taken from Floreen[11] and clearly shows the effect noted here. The more rapid increase of the 0.02% offset yield stress suggest the formation of an upper and lower yield stress. It should be noted that both measures of the yield stress continue to rise until the presence of reverted austenite begin to effect the data. Also, it should be observed that the U.T.S. is almost completely unaffected by this phenomenon.

Although no data is available concerning the toughness of ternary alloys after aging the implication here is clear. Although the cause of this effect is not known such aging treatments may represent a method of increasing the strength of an iron-nickel alloy in the absence of precipitation which is known to be detrimental to toughness.

IV. CONCLUSIONS

(1) Cryogenic alloy design utilizing a variant of the maraging steels proved to be a successful method of combining high strength and excellent toughness for low temperature application.

(2) An Fe-12Ni-4Co-2Mo-0.5Ti alloy subjected to a straightforward γ cycling procedure to reduce the prior austenitic grain size to $\sim$4-6 μm exhibited an excellent combination of strength and toughness at 77°K. The alloy had a yield strength of 151 ksi with a K_{IC}/σ_y ratio of 1.9 before aging and a yield strength of 162 ksi with a K_{IC}/σ_y ratio of 1.3 after aging.

(3) The same alloy subjected to a more complicated grain refinement involving miltiple 2 phase decomposition to produce a grain size of 1-2 μm exhibited a yield strength of 205 ksi at 4.2°K with a K_{IC}/σ_y ratio of 0.84 in the unaged condition. Aging produced a yield strength of 218 ksi but with a K_{IC}/σ_y ratio of only 0.425.

(4) Aging resulted in an increase in C_v energy for all test temperatures above the DBTT in both the γ cycled and C.R. structures.

(5) Aging at low temperatures was found to increase the yield point independently of the U.T.S. and introduced an upper and lower yield point. The cause for this effect was traced to the Fe-Ni "gettered" matrix but the mechanism remains unknown.

REFERENCES

1. G. R. Brophy and A. J. Miller, The Metallography and Heat Treatment of 8 to 10 Ni Steel, Trans. ASM 41, 1185 (1949).
2. C. L. Swales and A. G. Haynes, Role of Nickel Steels in LNG Tankers, Metal Progress 107, 43 (June 1975).
3. Data Book, Metal Progress 108, 118 (mid June 1975).
4. W. C. Marshall and R. F. Hehemann and A. R. Troiano, The Characteristics of 9% Ni Low Carbon Steel, Trans. ASM 55, 134 (1962).
5. H. Sussukida, T. Ando, and I. Tsuji, Characteristics of 9% Ni Steel for Low Temperature Service, Mitsubishi Heavy Industries Tech. Review 3, no. 4, 384 (1966).
6. W. P. Benter, Jr. and W. J. Murphy, Explosive-Bulge and Drop-Weight Tests of Quench and Tempered 9% Ni Steel, ASME, Petroleum Mechanical Engineering Conf., Philadelphia, Pa., Sept. 17-20, 1967.
7. W. A. Norwood, Factors Controlling the Fracture Toughness of Cryogenic Alloys (M.S. Thesis), LBL-1121, Dec. 1972.
8. S. Jin, J. W. Morris, Jr., and V. F. Zackay, An Iron-Nickel-Titanium Alloy with Outstanding Toughness at Cryogenic Temperature, in Advances in Cryogenic Engineering, ed. K. D. Timmerhaus (Plenum Press, New York, 1974), vol. 19, pp. 379-384.
9. S. Jin, J. W. Morris, Jr., and V. F. Zackay, Grain Refinement through Thermal Cycling in an Fe-Ni-Ti Cryogenic Alloy, in Technical Report No. 5, Office of Naval Research, Contract No. N00014-69-A-0200-1062, NR 031-762, January 1974.

10. S. Jin, S. K. Hwang, and J. W. Morris, Jr., Comparative Fracture Toughness Testing of Cryogenic Alloys at Liquid Helium Temperature, in Technical Report No. 5, Office of Naval Research, Contract No. N00014-69-A-0200-1062, NR 031-762, July 1974.

11. S. Floreen, H. W. Hayden, and T. M. Devine, Cleavage Initiation in Fe-Ni Alloys, Met. Trans. 2, 1403 (1971).

12. W. Jolley, Influence of a 3.20% Ni Addition on the Yield and Fracture Behavior of Alpha Iron, Trans. AIME 242, 306 (1968).

13. G. R. Speich and P. R. Swann, Yield Strength and Transformation Substructure of Quenched Iron-Nickel Alloys, J. Iron and Steel Inst., 480 (May 1965).

14. G. Saul, J. A. Roberson, and A. M. Adair, The Effect of Thermal Treatment on the Austenitic Grain Size and Mechanical Properties of 18% Ni Maraging Steels, Met. Trans. 1, 383 (1970).

15. W. C. Leslie and R. J. Sober, Yielding and Plastic Flow in a Polycrystalline "Interstitial Free" Fe-.15Ti Alloy, Trans. ASM 60, 99 (1967).

16. W. C. Leslie et al., Plastic Flow in Binary Substitutional Alloys of B.C.C. Iron - Effects of Strain Rate, Temperature, and Alloy Content, Trans. ASM 62, 690 (1969).

17. W. C. Leslie, Iron and Its Dilute Substitutional Solid Solutions, Met. Trans. 3, 5 (1972).

18. G. R. Speich et al., Strength and Toughness of Fe-10Ni Alloys Containing C, Cr, Mo, Co, Met. Trans. 4, 303 (1973).

19. K. Detert, Investigation of Transformation and Precipitation in 15% Ni Maraging Steels, Trans. ASM 59, 262 (1966).

20. J. M. Chilton and C. J. Barton, Identification of Strengthening ppts. in 18Ni (250) Al, V, Ti Maraging Steels, Trans. ASM 60, 528 (1967).

21. W. A. Spitzig, J. M. Chilton, and C. J. Barton, Structure and Strengthening Mechanisms in 300 Grade 18Ni-Co-Mo-Ti Maraging Steel, Trans. ASM 61, 635 (1968).

22. S. Floreen and G. R. Speich, Some Observations on the Strength and Toughness of Maraging Steels, Trans. ASM 57, 714 (1964).

23. D. T. Peters and C. R. Cupp, The Kinetics of Aging Reactions in 18% Ni Maraging Steels, Trans. Met. Soc. AIME 236, 1420 (1966).

24. S. Jin et al., A Simple Method for Charpy Impact Testing Below 6°K, in Advances in Cryogenic Engineering, ed. K. D. Timmerhaus (Plenum Press, New York, 1974), vol. 19, pp. 373-378.

25. F. J. Witt and T. R. Mager, A Procedure for Determining Bounding Values on Fracture Toughness K_{IC} at any Temperature, ORNL-TM-3894, (Oct. 1972).

26. P. C. Riccardella and J. L. Swedlow, A Combined Analytical-Experimental Fracture Study of the Two Leading Theories of Elastic-Plastic Fracture (J.-Integral and Equivalent Energy), Heavy Section Steel Technology Program, Technical Report No. 33, Westinghouse Electric Corp., WCAP-8224.

27. R. L. Miller, A Rapid X-Ray Method for the Determination of Retained Austenite, Trans. ASM 57, 892 (1964).

28. D. T. Peters and C. R. Cupp, The Kinetics of Aging Reactions in 18 Pct. Ni Maraging Steels, Trans. Met. Soc. AIME, 236, 1420 (1966).

29. S. K. Hwang, A Study on the Retained Austenite in Fine-Grained Fe-12Ni-0.25Ti Alloy (M.S. Thesis), LBL-3714, Feb. 1975.

30. M. Hanson, Constitution of Binary Alloys (McGraw-Hill, New York, 1958), p. 677.

31. R. L. Miller, Ultrafine-Grained Microstructures and Mechanical Properties of Alloy Steels, Met. Trans. 3, 905 (1972).

32. P. G. Shewmon, Transformations in Metals (McGraw-Hill, New York, 1969), p. 340.

LIST OF TABLES

Table 1. Cryogenic Alloy Mechanical Properties

Alloy	77°K				4-6°K			
	Y.S. (KSI)	U.T.S. (KSI)	C_v (ft-lb)	K_{IC} (KSI$\sqrt{in}$)	Y.S. (KSI)	U.T.S. (KSI)	C_v (ft-lb)	K_{IC} (KSI$\sqrt{in}$)
9 Ni Steel	146	172	92	168*	208	231	75	73
304 S.S.	81	235	128	213*	105	270	130	168*
12Ni-1/4Ti-Fe bal.	149	154	115	307*	195	219	99	232*

After S. Jin et al., Comparative Fracture Toughness Testing of Cryogenic Alloys at Liquid Helium Temperature Co.# N00014-69-A-0200-1062 NR 031-762 Tech. Rpt. #5

*Value calculated using equivalent energy concept.

XBL 758-6848

Table 2. Ingot Compositions*

Ingot No.	Ni	Co	Mo	Ti	C	O	N	P	S
‡749-26	12.08	3.97	2.07	0.03	†0.001	-	-	-	-
752-12	12.10	4.00	2.00	0.046	†0.001	0.060	0.001	0.008	0.004
‡749-24	12.03	N/A	N/A	0.01	†0.001	0.050	0.001	0.004	0.004
752-11	12.24	N/A	N/A	0.13	-	-	-	-	-
754-26	11.90	3.94	1.89	0.050	-	0.00[illegible]	-	0.010	-

*All values reported in wt. %
†less than
‡4 lb type ingot

XBL 758-6849

Table 3. Transformation temperature.

	As	Af	Ms	Mf
749-26*	690°C	742°C	460°C	431°C
749-24*	663°C	672°C	483°C	458°C

*Heating and cooling rate 10°C/min.

XBL '59-6850

Table 4. Tensile properties at 77°K.

As Quenched				Quenched and Tempered			
σy*	U.T.S.*	% Elong.	% R.A.	σy*	U.T.S.*	% Elong.	% R.A.
138.5	152.0	28.9	75.8	154/153	163.0	31.1	76.2

*Values reported in KSI.

XBL 758-6851

Table 5. Tensile properties, γ cycled structure.

	Solution Condition				Aged 444°C/4 hr/A.Q.			
Temp.	σy*	Tensile*	% Elong	% R.A.	σy*	Tensile*	% Elong	% R.A.
298°K	103.5	110.0	20.6	86.1	106.5	113	24	86.1
77°K	151	162.5	24.2	75.0	162/161	165.5	32.9	75.8
4.2°K**	205	218.6	17.9	67.2	212	226.5	21.9	69.5

*All values reported in KSI.

**Values based on one test. All others based on two.

XBL 758-6853

Table 6. Volume % austenite.*

Structure	298°K	77°K	4°K
Grain Refined Unaged	3%	2-1/2 %	1%

*Samples air cooled to R.T. and subjected to low temperature at some later time.

XBL 758-6852

Table 7. Tensile Properties, Grain Refined Structure

Temp.	Solution Condition				Aged 444°C/4 hrs/A.R.			
	σ_v*	Tensile*	% Elng.	% R.A.	σ_y*	Tensile*	% Elng	% R.A.
298°K	90.6	102	26.4	85.6	97.5/97.5	109	30.7	84.6
77°K	136.0	153	30.4	78.8	153/153	159	32.8	77.4
4.2°K	205	228	22.3	70.3	‡218.5	‡235	‡22.3	‡68.6

*All values reported in ksi

‡Values based on one test, all others based on two

XBL 758-6854

FIGURE CAPTIONS

Fig. 1. Showing dimensions of forged ingots and position of specimen.

Fig. 2. Heat treatment schematic.

Fig. 3. Diagram of round tensile specimen.

Fig. 4. Diagram of Charpy impact test specimen.

Fig. 5. Diagram of fracture toughness specimens.

Fig. 6. Aging curves plotting Rockwell hardness (A scale) vs. time (log) for 4Co-2Mo and 12Ni.

Fig. 7. Microstructure - Quench and Quench and Temper.

Fig. 8. Fractographs of Charpy specimens tested at 77°K and showing transgranular cleavage.

Fig. 9. Microstructure - γ cycled and γ cycled and aged structures.

Fig. 10. T.E.M. photomicrograph of γ cycled structure in unaged conditions.

Fig. 11. T.E.M. photomicrograph of γ cycled structure in unaged conditions.

Fig. 12. Fracture surface of Charpy specimen γ cycled in both unaged and aged condition tested at 77°K.

Fig. 13. Fracture toughness data of γ cycled and γ cycled and aged tested at 77°K.

Fig. 14. Fracture surface associated with fracture toughness tests above showing classical quasi cleavage fracture mode characteristic of high energy fracture.

Fig. 15. Photomicrographs of G.R. and G.R. and aged microstructure. 2000X mag.

Fig. 16. Plot of σ_y and U.T.S. vs. temperature for both aged and unaged structures.

Fig. 17. Charpy data plotted vs. temperature.

Fig. 18. Fracture toughness data from tests performed at 77°K.

Fig. 19. Fractographs of specimen surfaces tested at 77°K.

Fig. 20. Fracture toughness data from tests performed at 4°K.

Fig. 21. Fractographs of specimen surfaces tested at 4°K.

Fig. 22. Engineering stress-strain curve illustrating the effects of 444°C/4 hrs/Air Quench aging reaction.

Fig. 23. Plot of stress vs. 1 hr. aging temperature (after S. Floreen).

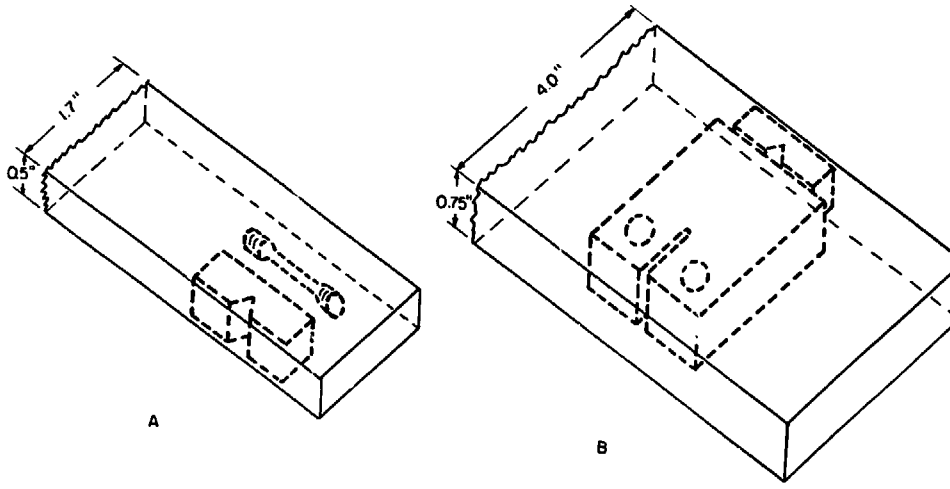

XBL 755-6274

Figure 1

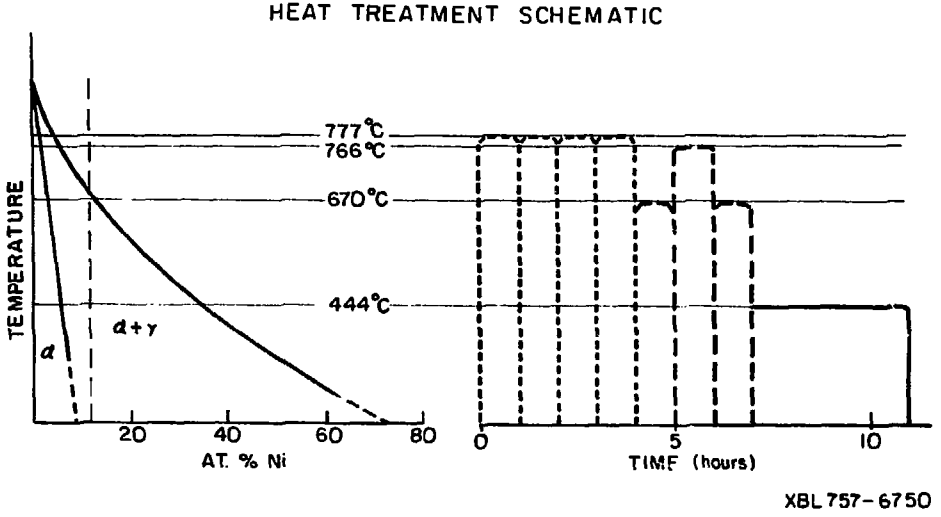
HEAT TREATMENT SCHEMATIC
TEMPERATURE
777°C
766°C
670°C
444°C
α+γ
α
20
40
60
80
AT. % Ni
0
5
10
TIME (hours)
XBL 757-6750

Figure 2

AS PER; ASTM DESIGNATION
E8-69

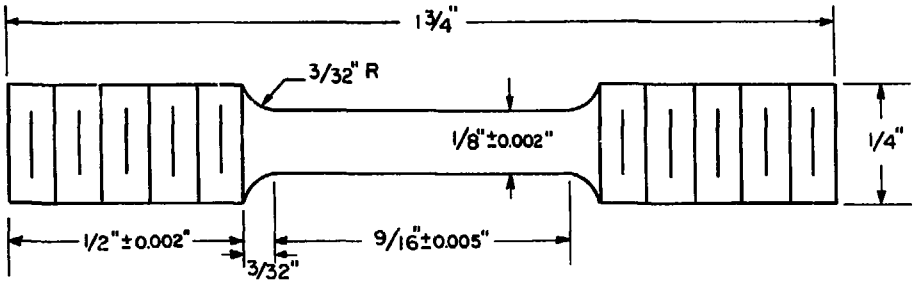

XBL755-6275

Figure 3

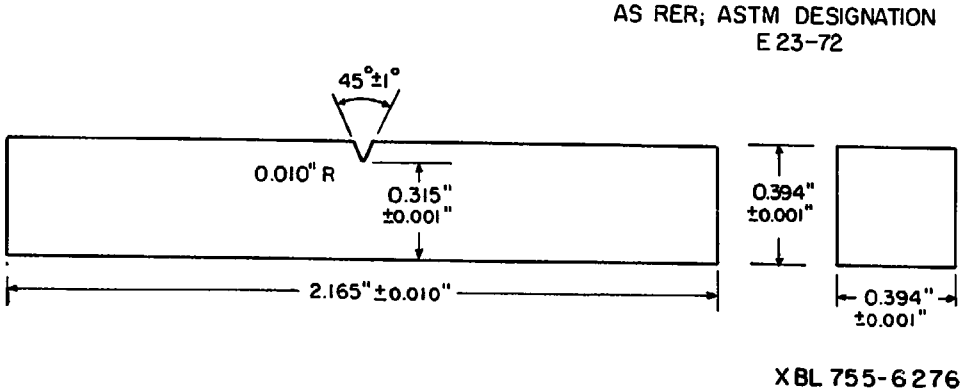
AS RER; ASTM DESIGNATION
E 23-72
45°±1°
0.010" R
0.315"
±0.001"
0.394"
±0.001"
2.165"±0.010"
0.394"
±0.001"
XBL 755-6276

Figure 4

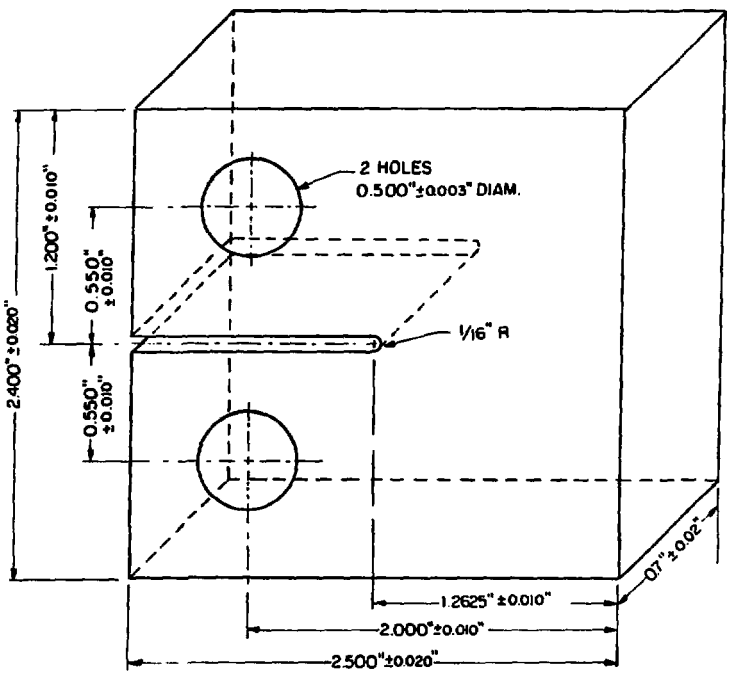
2 HOLES
0.500"±0.003" DIAM.
1/16" R
1.200"±0.010"
0.550"
±0.010"
0.550"
±0.010"
2.400"±0.020"
1.2625"±0.010"
2.000"±0.010"
2.500"±0.020"
.07"±0.02"
XBL 755-6277

Figure 5

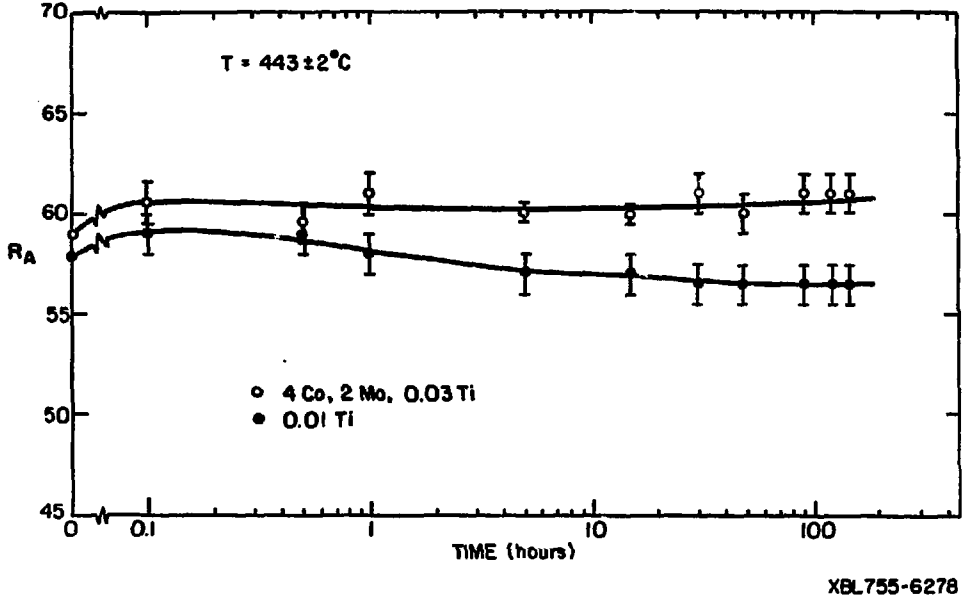
T = 443±2°C
70
65
60
55
50
45
R_A
0
0.1
1
10
100
TIME (hours)
4 Co, 2 Mo, 0.03 Ti
0.01 Ti
XBL755-6278

Figure 6

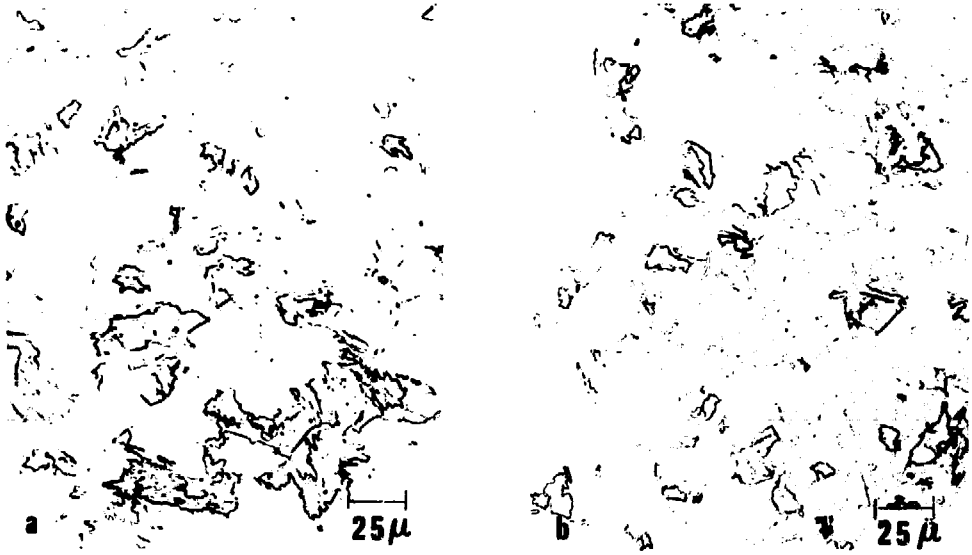

XBB 755-3477

Figure 7

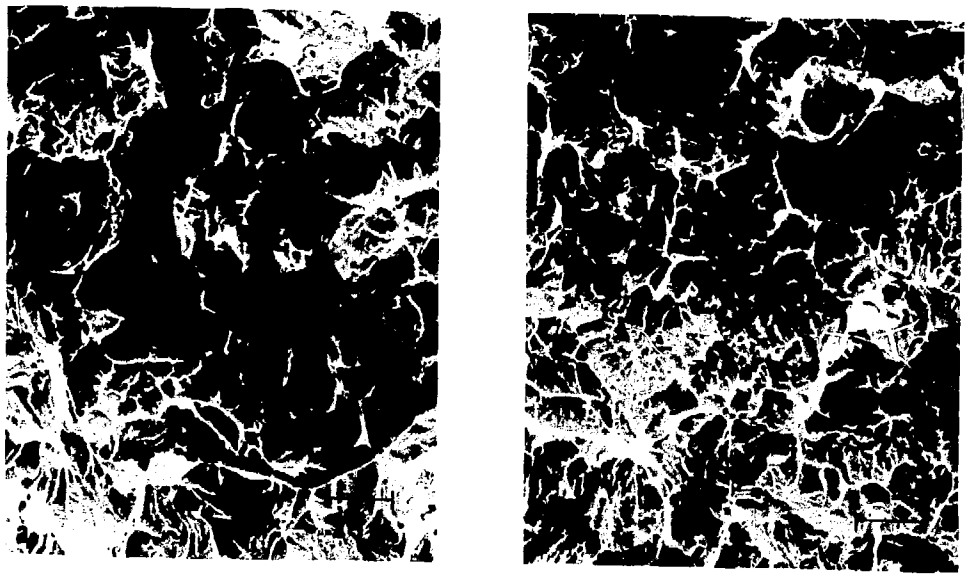

XBB 755-3476

Figure 8

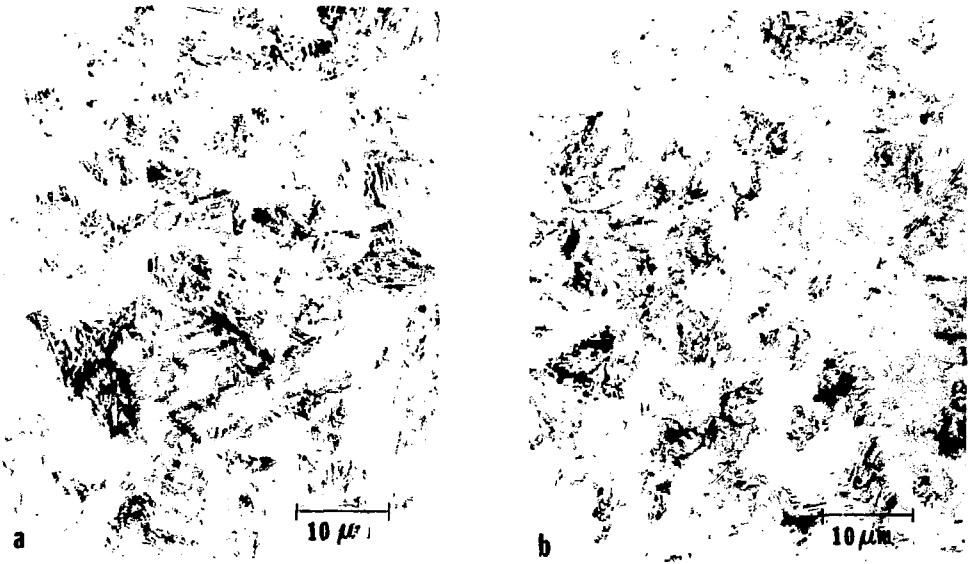

XBB 755-3478

Figure 9

XBB 755-6489

Figure 10

XBB 755-3473

Figure 11

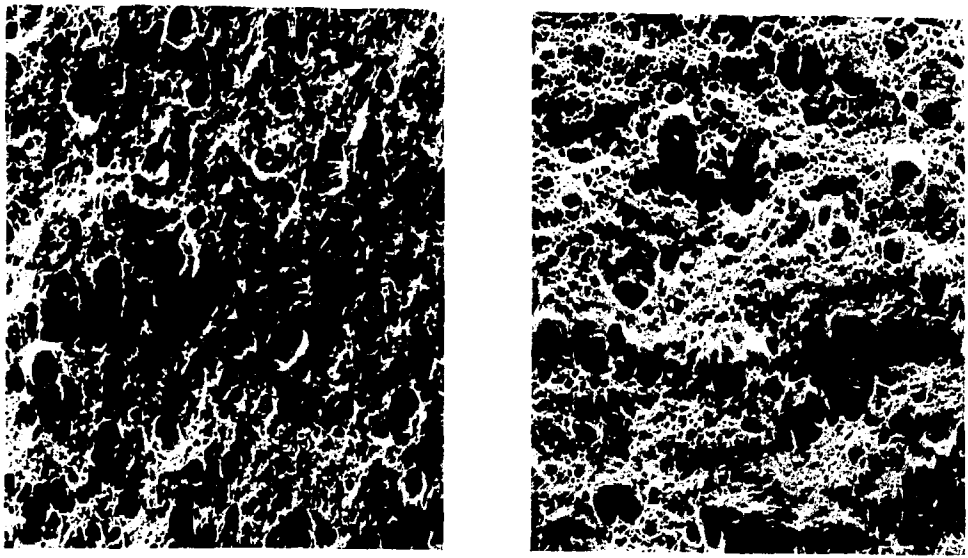

XBB 755-3475

Figure 12

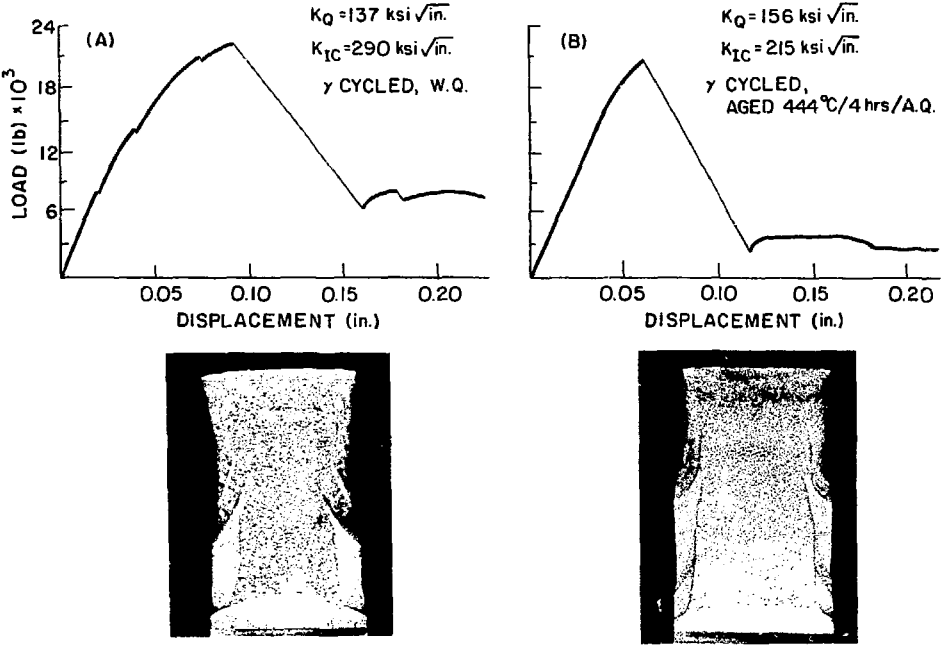

Figure 13

XBB 758-5780

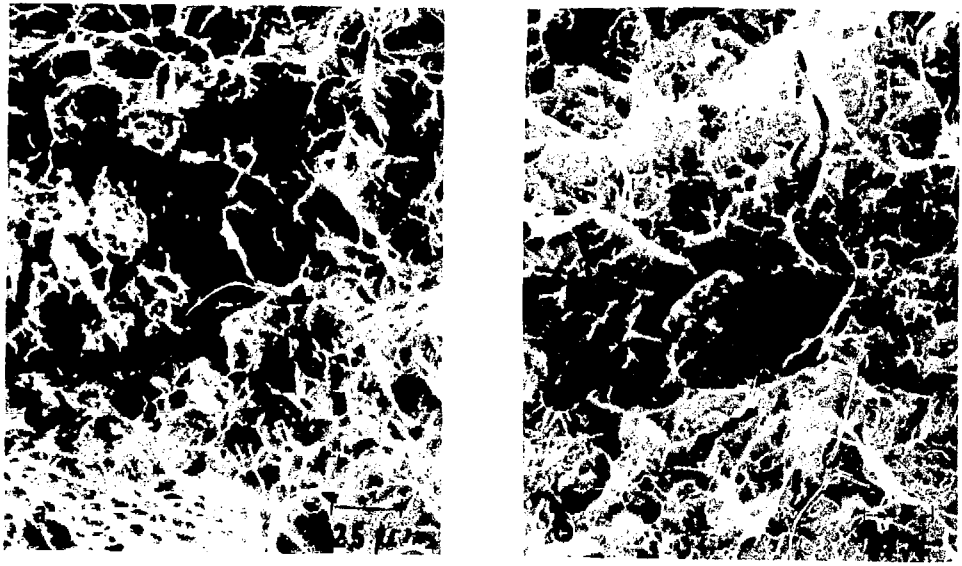

XBb 758-5775

Figure 14

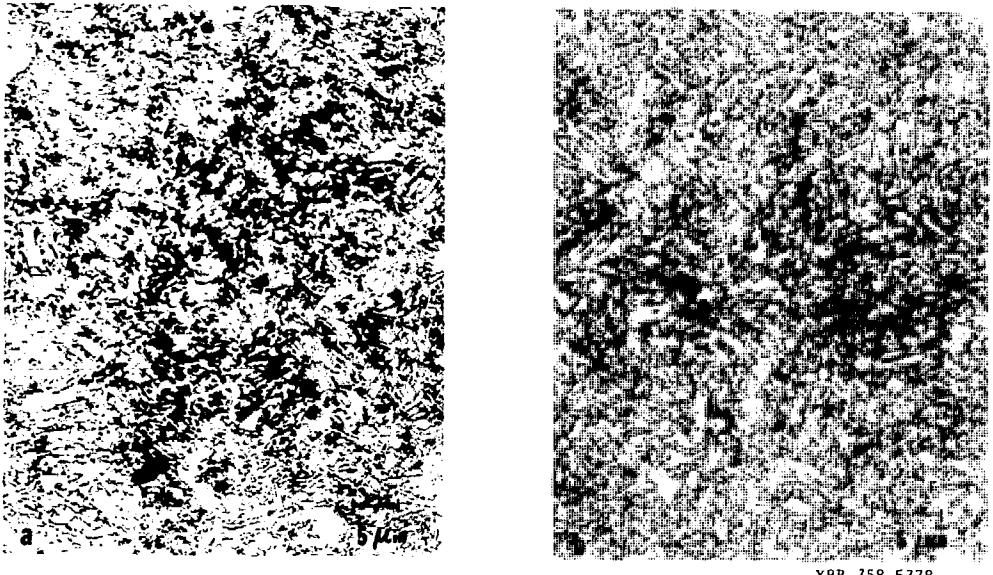

XBB 758-5778

Figure 15

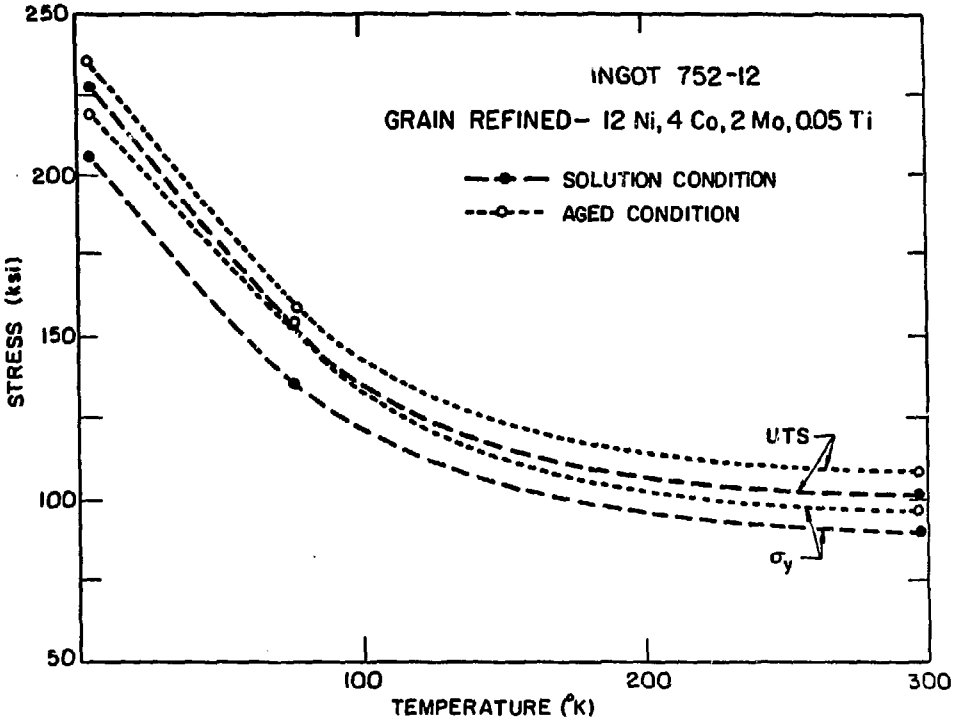
INGOT 752-12
GRAIN REFINED– 12 Ni, 4 Co, 2 Mo, 0.05 Ti
SOLUTION CONDITION
AGED CONDITION
UTS
σ_y
STRESS (ksi)
TEMPERATURE (°K)
250
200
150
100
50
100
200
300
XBL757-6752

Figure 16

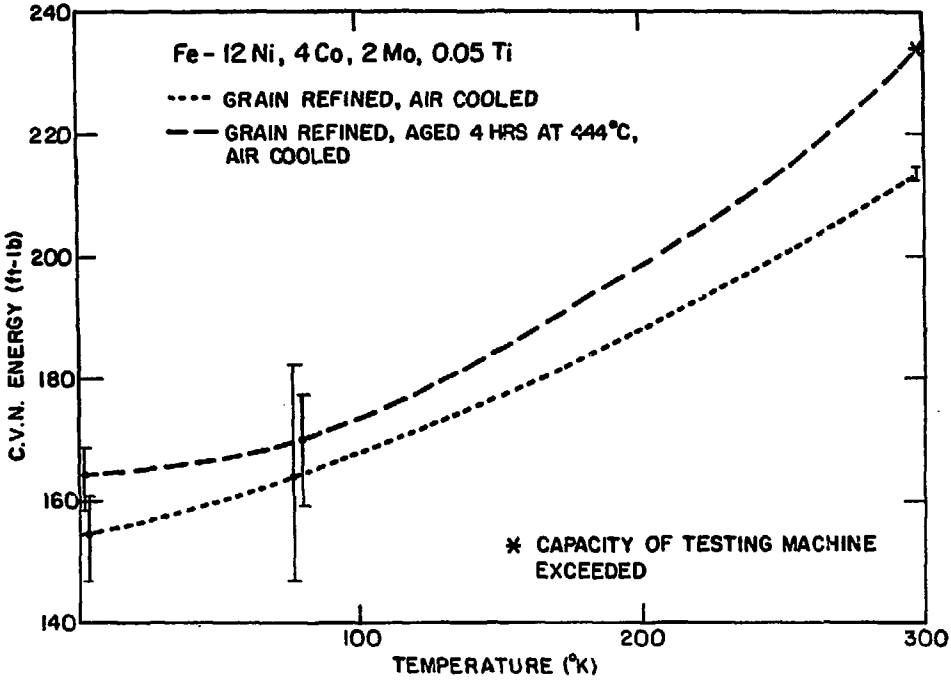
Fe - 12 Ni, 4 Co, 2 Mo, 0.05 Ti
---- GRAIN REFINED, AIR COOLED
— — GRAIN REFINED, AGED 4 HRS AT 444°C, AIR COOLED
* CAPACITY OF TESTING MACHINE EXCEEDED
C.V.N. ENERGY (ft-lb)
240
220
200
180
160
140
100
200
300
TEMPERATURE (°K)
XBL 757-6751

Figure 17

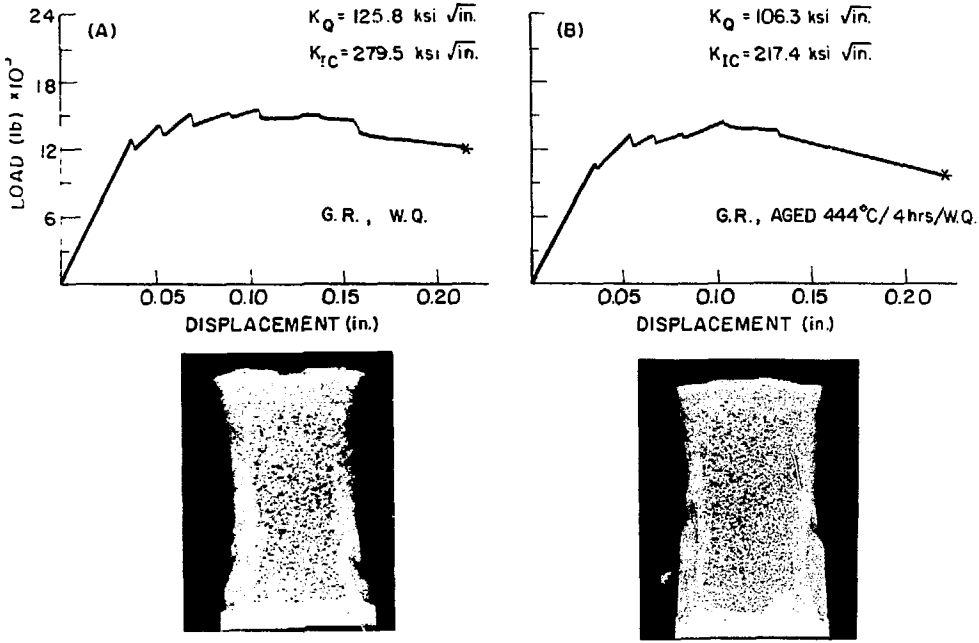

XBB 758-5781

Figure 18

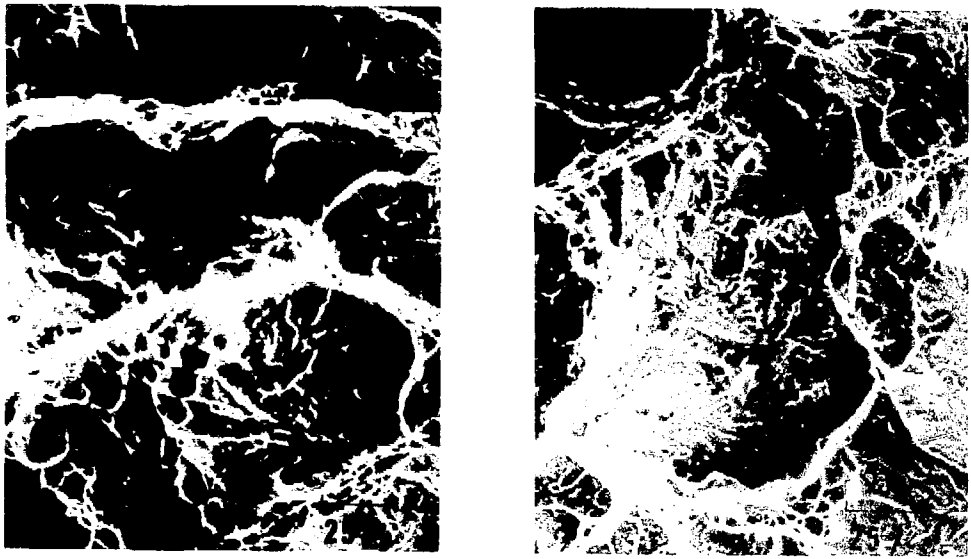

XBB 758-5777

Figure 19

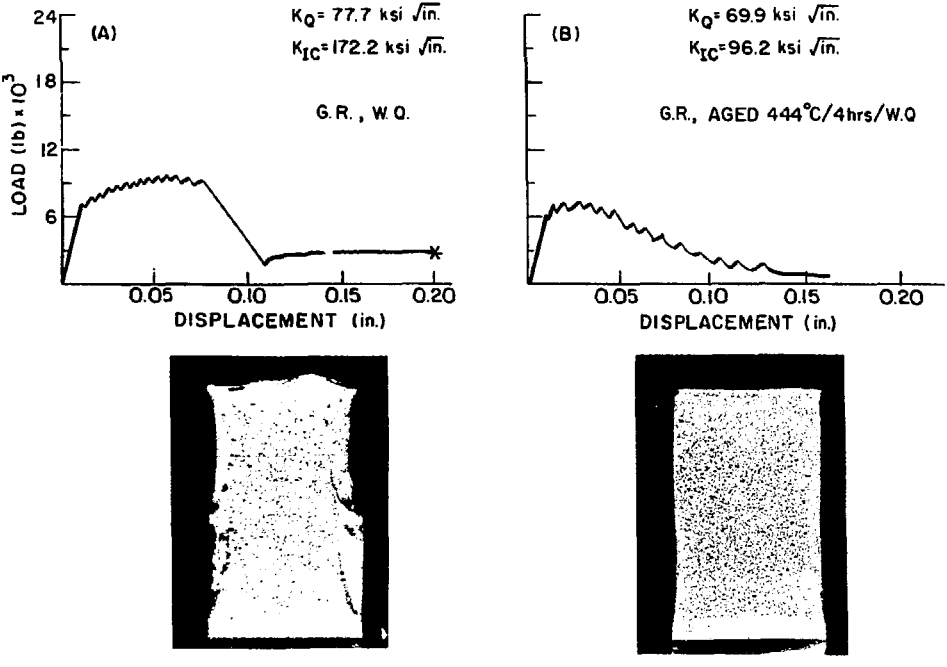
FRACTURE TOUGHNESS, 4°K
(A)
K_Q= 77.7 ksi $\sqrt{in.}$
K_{IC}=172.2 ksi $\sqrt{in.}$
G.R., W.Q.
LOAD (lb) x 10^3
24
18
12
6
0.05
0.10
0.15
0.20
DISPLACEMENT (in.)
(B)
K_Q= 69.9 ksi $\sqrt{in.}$
K_{IC}=96.2 ksi $\sqrt{in.}$
G.R., AGED 444°C/4hrs/W.Q
0.05
0.10
0.15
0.20
DISPLACEMENT (in.)

Figure 20

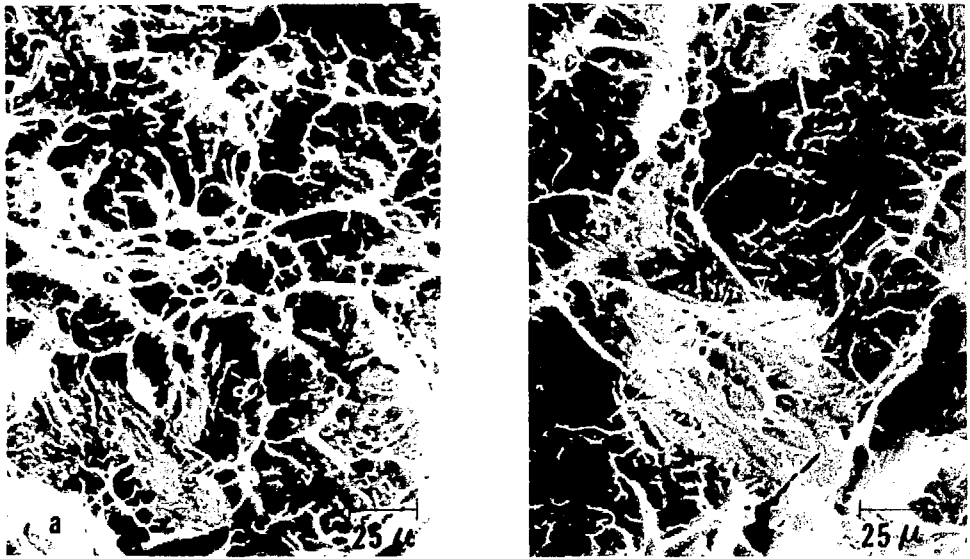

Figure 21

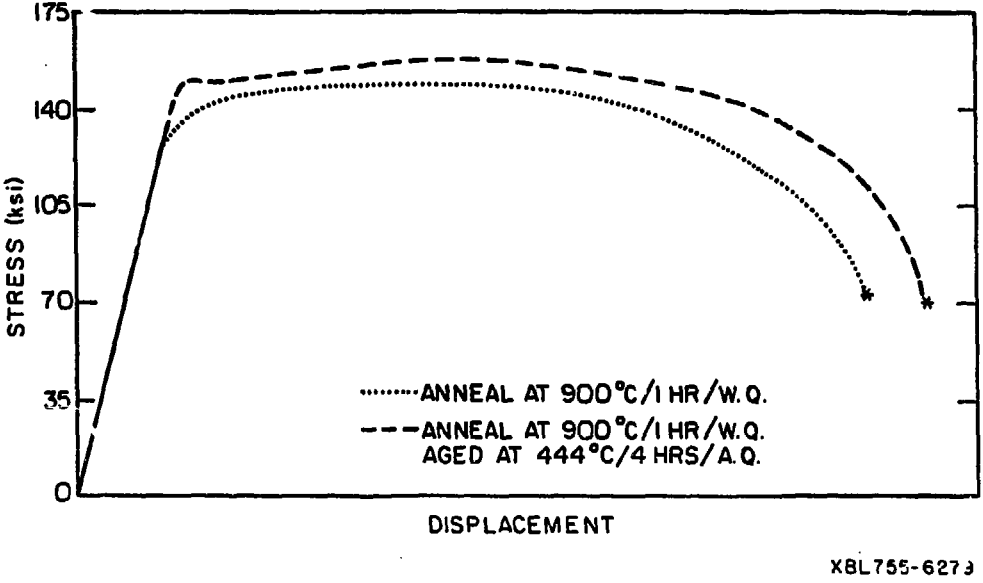
175
140
105
70
35
0
STRESS (ksi)
ANNEAL AT 900°C/1 HR/W.Q.
ANNEAL AT 900°C/1 HR/W.Q.
AGED AT 444°C/4 HRS/A.Q.
DISPLACEMENT
XBL755-6273

Figure 22

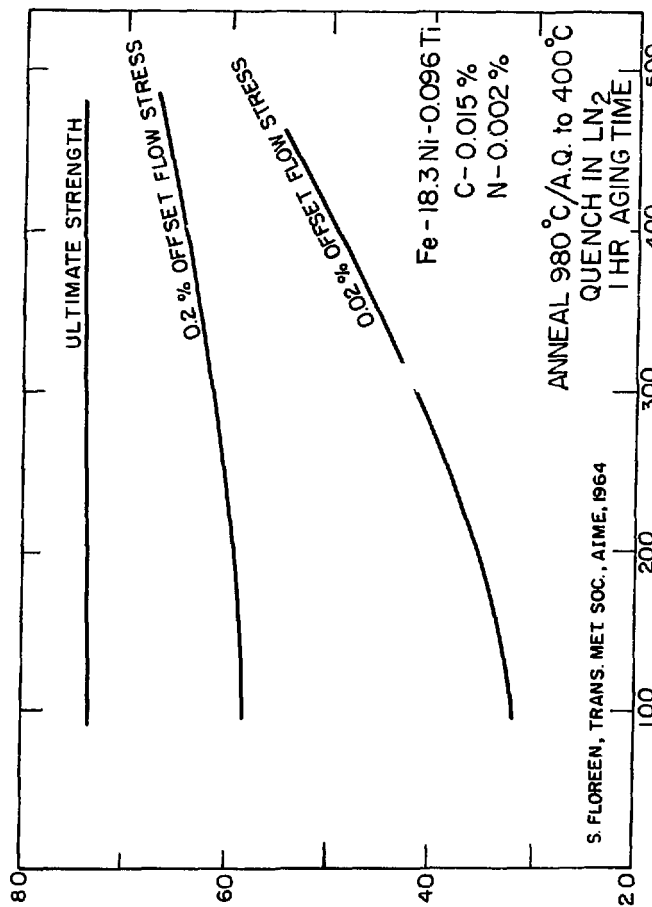

Figure 23

XBL 757-6753